MgB_2 under pressure: phonon calculations, Raman spectroscopy, and optical reflectance

INSTITUTE OF PHYSICS PUBLISHING JOURNAL OF PHYSICS: CONDENSED MATTER

J. Phys.: Condens. Matter **13** (2001) 9945–9962 PII: S0953-8984(01)25323-5

MgB_2 under pressure: phonon calculations, Raman spectroscopy, and optical reflectance

K Kunc[1], I Loa[2], K Syassen, R K Kremer and K Ahn

Max-Planck-Institut für Festkörperforschung, Heisenbergstrasse 1, D-70569 Stuttgart, Germany

E-mail: i.loa@fkf.mpg.de

Received 30 May 2001, in final form 17 August 2001
Published 19 October 2001
Online at stacks.iop.org/JPhysCM/13/9945

Abstract

The effect of pressure on optical phonon frequencies of MgB_2 has been calculated using the frozen-phonon approach based on a pseudopotential method. Grüneisen parameters of the harmonic mode frequencies are reported for the high-frequency zone-centre E_{2g} and B_{1g} and the zone-boundary E_{2u} and B_{2u} modes at A. Anharmonic effects of phonon frequencies and the implications of the calculated phonon frequency shifts for the pressure dependence of the superconducting transition temperature of MgB_2 are discussed. Also reported are Raman and optical reflectance spectra of MgB_2 measured at high pressures. The experimental observations in combination with calculated results indicate that the broad spectral features that we observed in the Raman spectra at frequencies between 500 and 900 cm^{-1} cannot be attributed to first-order scattering by zone-centre modes, but originate in part from a chemical species other than MgB_2 at the sample surface and in part from a maximum in the MgB_2 phonon density of states. Low-temperature Raman spectra taken at ambient pressure showed increased scattering intensity in the region below 300 cm^{-1}.

1. Introduction

Magnesium diboride, MgB_2, was recently discovered to exhibit a superconducting transition at 39 K [1], which is by far the highest T_c for a binary compound. The light atomic masses in MgB_2 enhance the phonon frequencies which set the scale for T_c in Bardeen–Cooper–Schrieffer (BCS) theory. A variety of experimental observations (e.g., isotope effects [2] and scanning tunnelling measurements of the superconducting gap [3–5]), indeed indicate phonon-mediated (BCS) superconductivity, and theory finds medium or strong electron–phonon coupling [6–9].

[1] Permanent address: CNRS and Université Pierre et Marie Curie, Laboratoire d'Optique des Solides UMR7601, T13-C80, 4 place Jussieu, 75252 Paris Cédex 05, France.
[2] Author to whom any correspondence should be addressed.

0953-8984/01/449945+18$30.00

The coupling is predicted to be particularly strong for the zone-centre optical phonon of E_{2g} symmetry and the related phonon branch connecting to the zone-boundary E_{2u} mode at the A point (the direction along the c-axis of the AlB_2-type structure) [7–9].

The effect of pressure on the superconducting properties of MgB_2 has been studied by several groups [10–15]. While there is some scatter in the experimental pressure coefficients, all studies show a decrease of T_c, at rates between 0.7 and 2.0 K GPa^{-1}. Lattice parameters under pressure have been determined by means of neutron and x-ray diffraction [16–19]. An *ab initio* calculation of the pressure–volume relation and the optimized c/a axial ratio under pressure [20] is in good agreement with the experimental data. It was concluded that the decrease in T_c is not driven by a change in the electronic density of states near E_F but by an increase in phonon frequencies, specifically of the strongly coupled E_{2g} mode [20].

The frequency of the $E_{2g}(\Gamma)$ phonon is expected to be between 486 and 665 cm^{-1}, according to recent calculations [6, 8, 9, 21, 22]. So far, this phonon mode has not been identified unambiguously by means of neutron inelastic scattering [9, 23, 24] or in Raman experiments [19, 22, 25–27]. A Raman spectrum taken by Bohnen *et al* [22] indicates a broad asymmetric feature near 580 cm^{-1}, while other authors [19, 26, 27] report an even broader feature (260–300 cm^{-1} width) centred near 620 cm^{-1}. Contradictorily, compliance with the selection rules for an E_{2g} mode has been reported [27] as well as complete breakdown of the same, attributed to resonance effects [26]. The 620 cm^{-1} feature was observed to increase in frequency under pressure, with an unusually large Grüneisen parameter [19]. It was generally assigned to first-order zone-centre phonon scattering, highly broadened by strong electron–phonon coupling or anharmonic effects, but other interpretations were also considered.

In this paper we present a theoretical investigation of the pressure dependence of phonon frequencies of MgB_2. As no phonon has been, so far, unambiguously identified experimentally, the theoretical methods gain in importance—in particular the *ab initio* approaches, such as the frozen-phonon method which is employed in this work. Compared to linear response theory, the frozen-phonon method has the disadvantage that it is not very efficient in generating an overall picture of the phonon dispersions throughout the Brillouin zone, but is restricted to calculation of a few high-symmetry modes. One of the advantages of the frozen-phonon method, however, is that it yields information on anharmonic effects, which in earlier calculations [9] were found to be particularly large for the atomic displacements corresponding to the E_{2g} mode of MgB_2. The immediate interest in the shifts of phonon frequencies is in the context of interpreting the pressure dependence of T_c. Furthermore, the calculated pressure dependences of phonon frequencies can in principle be useful for the identification of spectral features in Raman spectra.

We also report here Raman and optical reflectance measurements of MgB_2 as a function of pressure at room temperature. On the basis of the pressure dependence of Raman spectra and the optical reflectance and by taking into account the results of the phonon frequency calculations, we argue that the observed Raman features are not due to zone-centre first-order Raman scattering from MgB_2. The interpretation that we suggest for our Raman results considers a superposition of a density-of-states peak of MgB_2 and scattering by a different chemical species present at the surface of as-grown samples. We also take a look at zero-pressure Raman spectra measured as a function of temperature in order to check whether it is possible to observe a pair-breaking excitation below T_c.

The paper is organized as follows. The symmetry analysis of all phonon modes at the Γ and A points is presented in section 2. Details of the theoretical method and the calculated results are presented and discussed in section 3. Experimental details and results are given in section 4, followed by conclusions in section 5.

2. Symmetry analysis

The frozen-phonon calculations described below require knowledge of the phonon displacement patterns. We thus start with the symmetry analysis of the vibrational spectra. The point group of the AlB_2 structure is D_{6h}. A factor-group analysis yields the decomposition of the coordinate representation

$$B_{1g} + E_{2g} + 2A_{2u} + 2E_{1u} \qquad \text{at } \Gamma \tag{1}$$

and

$$A_{1g} + E_{1g} + A_{2u} + B_{2u} + E_{1u} + E_{2u} \qquad \text{at A} \tag{2}$$

with, at the point Γ, one A_{2u} and one E_{1u} referring to the rigid translations ($\omega = 0$). Constructing then projection operators we find the bases spanning the irreducible representations in equations (1) and (2)—i.e., the respective phonon displacement patterns at Γ and A, respectively. They are shown in figures 1 and 2, with the modes arranged (columnwise) in the order of decreasing MgB_2 eigenfrequencies (which are obtained later, in section 2.3). At high pressures this ordering may, of course, be altered. The patterns in figure 2 are arranged

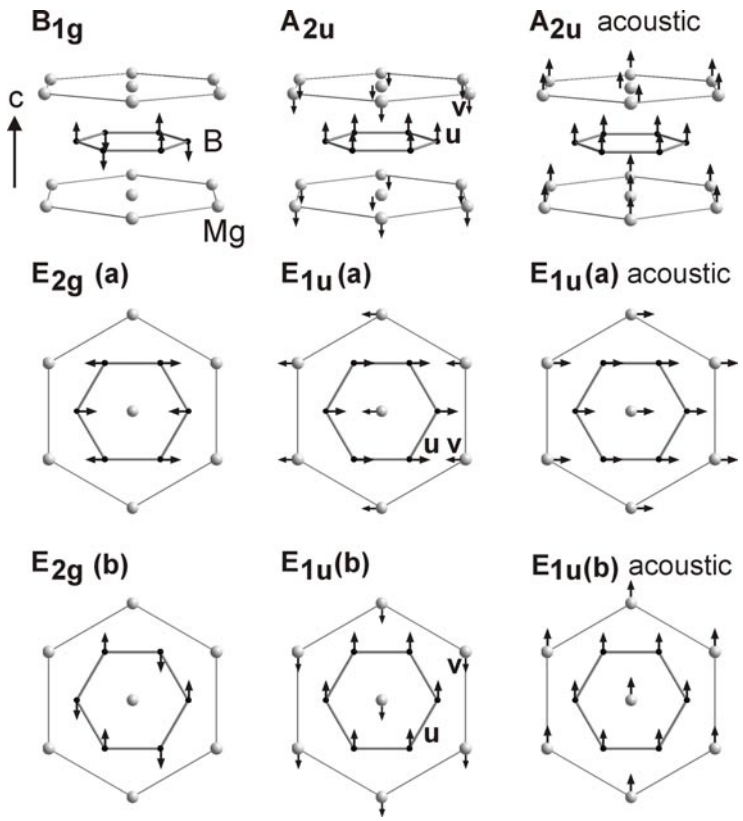

Figure 1. Phonon displacement patterns of the zone-centre (Γ) modes in MgB_2 (the AlB_2 structure, point group D_{6h}), in the order of decreasing frequencies (at zero pressure, columnwise). The labels (a), (b) denote the different patterns corresponding to the degenerate E modes. For the (optic) A_{2u} and E_{1u} patterns to be eigenmodes, the displacements u, v of the two sublattices have to be such that the unit cell's centre of mass stays at rest, i.e. $u{:}v = M_{Mg}{:}2M_B$. The E_{2g} mode is Raman active, the A_{2u} and E_{1u} modes infrared active, and the B_{1g} mode silent.

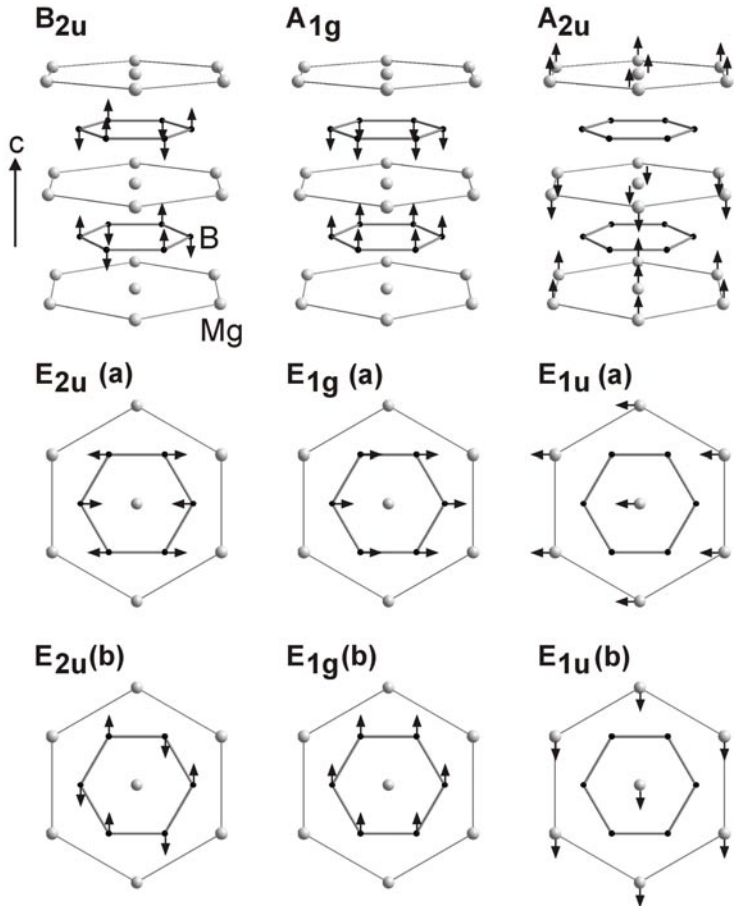

Figure 2. Symmetry-determined displacement patterns for the zone-boundary modes at the A point of the hexagonal Brillouin zone. Only one layer of MgB_2 is shown in the E patterns, and it is understood that equivalent atoms above and below the layer displayed vibrate in opposite directions. The patterns are arranged so as to belong to the same branch of the phonon dispersion $\omega_j(\vec{k})$ as the corresponding Γ modes in figure 1; thus e.g. the three patterns in the last column are the 'end-points' of the acoustic branches.

so as to be the 'end-points' of those Γ–A branches of the phonon dispersion that start with the corresponding pattern in figure 1. This means that e.g. the three patterns in the last column of figure 2 are the end-points of the acoustic branches.

The patterns at A alternate the $+u$- and $-u$-displacements from one layer to another. In addition, for the two highest-frequency modes we notice that (to within the ± alternation) the patterns of a layer are the same as at Γ.

3. Calculations

3.1. Theoretical method

The frozen-phonon approach starts from the *ab initio* evaluation of the total energy E^{tot} of the solid with frozen-in atomic displacements. The energy is evaluated using the density

functional theory (DFT) within the generalized gradient approximation (GGA) [28]. We work in a plane-wave basis and use pseudopotentials. For the actual calculations we employed the VASP codes [29–32], and the ultrasoft Vanderbilt-type pseudopotentials [33] were supplied by Kresse and Hafner [34]. The pseudopotential that we chose for Mg treats the semi-core states explicitly, i.e., Mg is represented with eight valence electrons, $2p^6 3s^2$, and the non-linear core correction (NLCC) [35] is applied as well. The calculations are carried out with the plane-wave cut-off energy of 33.6 Ryd, and the Brillouin zone sampling is based on Γ-centred uniform meshes $16 \times 16 \times 14$ or $16 \times 16 \times 8$—the latter one applied in the calculations with the doubled unit cell for frozen phonons at the Brillouin zone boundary. As the system is metallic, the $\vec{k}$-space integration with the incompletely filled orbitals uses the tetrahedron method [36] with Blöchl's corrections [37]. The above meshes divide the Brillouin zone into 21 504 or 12 288 tetrahedra; the number of *irreducible* tetrahedra is lower by a factor 2 to 6, depending on the symmetry of the frozen-in phonon.

3.2. Structural properties

For eleven volumes between 25.0 Å^3 and 29.6 Å^3, we calculated $E^{tot}(V)$ with different c/a values while keeping the volume V constant and, for every chosen V, found the optimized structure, i.e. the corresponding $a(V)$, $c(V)$, $c/a(V)$, and $E(V)$. The latter data were fitted by the Murnaghan relation for $E(V)$ [38]

$$E(V) = E_0 + \frac{B_0 V_0}{B'}\left[\frac{V}{V_0} + \frac{(V/V_0)^{1-B'} - B'}{B'-1}\right] \tag{3}$$

which provided the static equilibrium[3] as well as the bulk modulus B_0 and its pressure derivative B'. The results are summarized in table 1. The calculated equilibrium volume ($V_0 =$ 28.663 Å^3) compares well with the experimental value $V_0 = 28.917(1)$ Å^3 (reference [18], at 37 K) meaning that we are -0.9% off in V_0. The individual lattice parameters are -0.6% off the experimental result for a_0, +0.2% for c_0, and +0.8 % for c_0/a_0. The variation of c/a under pressure has been translated into a quadratic function of $1 - V/V_0$ and its coefficients are given in table 1 as well. The present results are also in good agreement with those of a previous calculation [20] (see table 1).

Table 1. Calculated structural parameters of MgB_2 at zero pressure: equilibrium volume (V_0), lattice constants (a_0, c_0), bulk modulus (B_0), and its pressure derivative (B'). The variation of the calculated c/a ratio with volume is given by the quadratic polynomial $c/a = c_0/a_0 + \alpha(1 - V/V_0) + \beta(1 - V/V_0)^2$ with the coefficients α, β listed below.

	V_0 (Å^3)	a_0 (Å)	c_0 (Å)	B_0 (GPa)	B'	c_0/a_0	α	β
Present calculation	28.663	3.065	3.522	144.7	3.6	1.1490	−0.258	−0.06
FP-LAPW calculation [20]	28.888	3.075	3.527	140.1	3.93	1.1468	−0.211	−0.272
Experiment	28.917(1)[a]	3.08230(2)[a]	3.51461(5)[a]	147–155[b]	(4.0[b])	1.14026[a]		

[a] Reference [18], at 37 K.
[b] References [16, 18, 19] with the *assumption* that $B' = 4$.

A limited testing of different pseudopotentials revealed that treating the magnesium $2p^6$ electrons as valence states is *not* essential for getting the correct equilibrium, but using the GGA

[3] Only data from the interval $V = (26.8, 29.6)$ Å^3 were used for determination of static equilibrium; the remaining ones ($V < 26.8$) provide an independent check.

(rather than the LDA) *is* essential[4]. With the value of $c/a = 1.14$ the MgB_2 is well inside the stability region of the AlB_2 structures [39]. A rather high pressure would probably be required to induce a phase transition, possibly towards the UHg_2-type structure (isostructural to AlB_2, but c/a less than $\sim$0.8) or a variant thereof, as is observed in other AlB_2-type intermetallic compounds [40].

The subsequent calculations of phonon frequencies are performed at the *calculated* equilibrium, and at volumes related to pressure by the P–V Murnaghan relation

$$P(V) = \frac{B_0}{B'}\left[(V/V_0)^{-B'} - 1\right] \tag{4}$$

which uses the *calculated* V_0, B_0, B' quoted in table 1.

3.3. Phonon frequencies

In this work we are mainly concerned with the two highest-frequency modes $B_{1g}(\Gamma)$ and $E_{2g}(\Gamma)$ and their A-point counterparts $B_{2u}(A)$ and $E_{2u}(A)$. For comparison with previous works we calculated the $A_{2u}(\Gamma)$ and $E_{1u}(\Gamma)$ as well. The branch $E_{2g}(\Gamma)$–$E_{2u}(A)$ in the phonon dispersion is the one that exhibits the strongest electron–phonon coupling [8], and $B_{1g}(\Gamma)$ is the z-displacement analogue of $E_{2g}(\Gamma)$.

We determine the vibrational eigenfrequencies using the frozen-phonon method [41], while paying particular attention to obtaining the *harmonic* part of the *ab initio* calculated energy differences that, inevitably, have to be probed by means of *finite* displacements u. Thus for each pattern, atoms are given five different displacements ranging from $u/a = 0.010$ to 0.035, and the (six) calculated energy values $E(u)$ are fitted with a quartic polynomial yielding

$$\Delta E_{tot}(u) = a_2(u/a)^2 + a_3(u/a)^3 + a_4(u/a)^4. \tag{5}$$

As an example we show in figure 3 the variation of $E_{tot}(u)$ for the $E_{2g}(\Gamma)$ mode[5]. The harmonic part of ΔE_{tot} is then retained for determination of the phonon energy:

$$\frac{\omega^2}{2}\sum M_\kappa u_\kappa^2 = E^{harm}(u \neq 0) - E^{harm}(u = 0). \tag{6}$$

For the four phonons listed above the procedure is repeated at various volumes. Although straightforward, this procedure calls for some explanation.

The frozen-in phonon displacements of figure 1 conserve the translational symmetry of the elementary unit cell defining the MgB_2 structure. With the zone-boundary modes given in figure 2 the total-energy calculations as a function of displacement u are to be done on a unit cell obtained by *doubling* the elementary cell (i.e. along the [001] direction), which then comprises two formula units of MgB_2. The frozen-in displacements also lower the rotational symmetry of the system: starting from D_{6h}, which is the point group of the MgB_2 lattice, we end up with, respectively, D_{3d}, D_{2h}, C_{2h} when the $B_{1g}(\Gamma)$, $E_{2g}(\Gamma)$-(a), $E_{2g}(\Gamma)$-(b) displacements are imposed, and D_{3h}, D_{2h}, D_{2h} with the $B_{2u}(A)$, $E_{2u}(A)$-(a), $E_{2u}(A)$-(b) displacements, respectively.

As the displacements u are finite, a larger or smaller degree of anharmonicity will always be present, but some restrictions on the latter can be read out from symmetry. With all patterns at the zone boundary, replacing $+u$ by $-u$ has the same effect as shifting the phonon-distorted structure by the lattice constant c, and it leaves $E(u)$ invariant. Consequently, the cubic (and,

[4] Within the LDA (i.e. without the GGA), we obtained $V_0^{th} = 27.371$ with $2p^6$ treated as valence electrons and $V_0^{th} = 27.421$ without the $2p^6$: -5.3% off the experimental value.

[5] The detailed exploration of $E(u)$ at very small displacements ($|u/a| < 0.010$) was carried out for the $E_{2g}(\Gamma)$-(b) mode only.

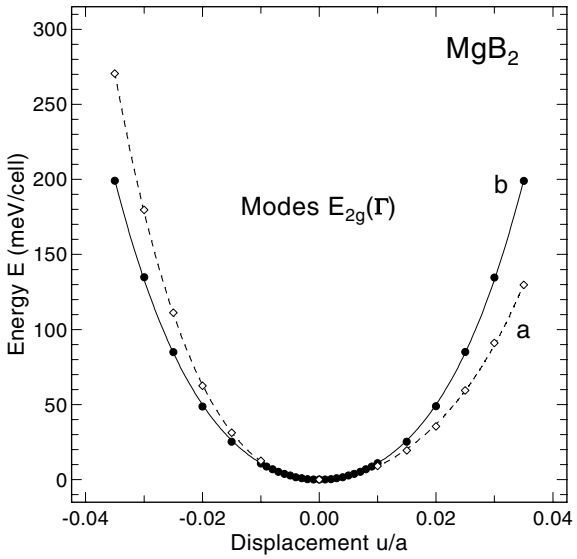

Figure 3. Calculated total energy of MgB_2 at equilibrium volume as a function of boron displacements corresponding to the $E_{2g}(\Gamma)$-(a) and $E_{2g}(\Gamma)$-(b) modes of figure 1. Full circles and open diamonds: *ab initio* total-energy calculations; solid and dashed lines: quartic polynomials, equation (5).

generally, odd-power) anharmonicity is forbidden in all zone-boundary modes. Inspecting, in turn, the displacement patterns for Γ, we realize that for nearly all modes the $+u \leftrightarrow -u$ substitution is equivalent to applying a mirror reflection or C_2 rotation—an operation which, in spite of the lowered symmetry, is still present in the point groups of the phonon-modulated structures—and which thus leaves invariant the structure and its energy $E(u)$. This forbids the cubic term in the expansion of $E(u)$ as well. Among the nine modes in figure 1 the $E_{2g}(\Gamma)$-(a) pattern is the only one in which all anharmonic terms are allowed and in which the cubic anharmonicity is to be expected.

For evaluation of phonon frequencies from $\Delta E_{tot}(u)$ we used the atomic masses of B and Mg that correspond to the natural isotope distribution: 10.8 and 24.3 amu; this is the usual approach in the spirit of the virtual-crystal approximation. We should keep in mind that for a ^{10}B-enriched sample the frequencies of all the modes involving boron would be higher by 4%.

Table 2 summarizes the results of our frozen-phonon calculations at different volumes: the variations with volume or pressure are described by the mode Grüneisen parameter, namely $\gamma_0 = -[\mathrm{d} \ln \omega / \mathrm{d} \ln V]_{V_0}$, or the coefficients a and b of a quadratic fit (see the caption). Figure 4 shows the calculated phonon frequencies as a function of volume.

We estimate that the calculated harmonic frequencies are uncertain to ∼1–3% (depending on the mode); this is the 'instrumental precision' of the determination of total energies and the uncertainty following from the error analysis in fitting the variations $E(u)$ by polynomials.

3.4. Anharmonicity and the $E_{2g}(\Gamma)$ mode

We note that the five displacements u/a quoted above range from half to approximately double the r.m.s. displacement [7], and one expects vibrations in both harmonic and anharmonic regimes. The effort of removing the anharmonic contributions from ΔE_{tot} yields, in turn, an insight into the anharmonicities.

Table 2. Calculated pressure and volume dependence of selected phonon frequencies in MgB_2. The zero-pressure frequency ω_0 and the linear and quadratic pressure coefficients were obtained from least-square fits of $\omega(P) = \omega_0 + aP + bP^2$ to the calculated data, and the mode Grüneisen parameters γ_0 (at equilibrium volume) are derived from a similar quadratic expression for $\omega(V)$. P has been obtained from V through the calculated P–V relation (see the text).

Mode	ω_0 (cm^{-1})	a (cm^{-1} GPa^{-1})	b (cm^{-1} GPa^{-2})	γ_0
$B_{1g}(\Gamma)$	695	3.06506	−0.018995	0.6
$E_{2g}(\Gamma)$	535	8.9744	−0.0780	2.5
$B_{2u}(A)$	636	1.70378	−0.01163	0.4
$E_{2u}(A)$	480	8.9019	−0.0809	2.8

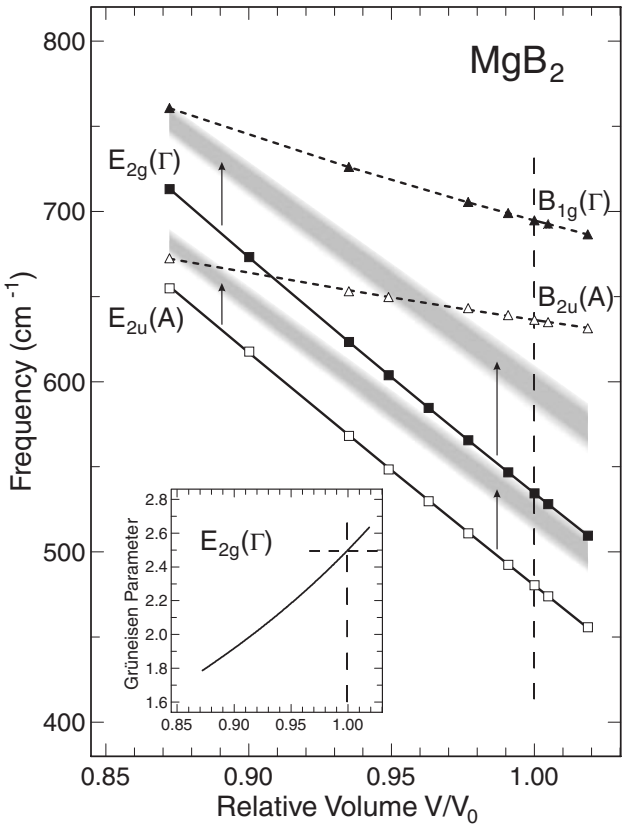

Figure 4. Calculated harmonic frequencies of the two highest modes at Γ and A in MgB_2 as a function of relative volume; V_0 refers to calculated static equilibrium (zero pressure). The lines represent quadratic relations fitted to the calculated points, and they define the mode Grüneisen parameters γ_0 listed in table 1. Note that γ itself depends on pressure; its variation with volume is shown in the inset. The shaded areas represent estimates for the $E_{2g}(\Gamma)$ and $E_{2u}(A)$ frequencies taking into account anharmonic corrections, as given by Yildirim *et al* [9] and scaled with the present values for the quartic coefficient in equation (5). (The widths of these areas reflect the uncertainties inherent to the estimates—see the text.)

The phonons exhibiting the strongest electron–phonon coupling are those of the $E_{2g}(\Gamma)$–$E_{2u}(A)$ branch [8]. $E_{2g}(\Gamma)$ has already received considerable attention [6, 8, 9, 21, 22]. Being

doubly degenerate, it is constituted by *two* distinct displacement patterns which are labelled (a) and (b) in figure 1. They should both lead to the same eigenfrequency (the same coefficient a_2 in equation (5)) and, in this sense, they are equivalent—as long as we stay within the harmonic approximation, i.e., within the standard group-theory reasoning. Once we step out of the harmonic approximation, the displacements (a) and (b) will become two unrelated patterns which are described by different anharmonic coefficients. This is confirmed by numerical calculations and we obtained $a_2 = 107$ eV/cell with both (a) and (b) patterns and, somewhat unexpectedly, also $a_4 = 45800$ eV/cell, equal for *the two* patterns. The two modes are nevertheless distinct as regards the cubic term, which is absent in the (b) pattern ($a_3 = 0$) and given by $a_3 = -1644$ eV/cell in the (a) pattern.

It is not difficult to understand why the mode $E_{2g}(\Gamma)$-(a) exhibits a strong cubic anharmonicity: giving the boron atoms a $+u$- or $-u$-displacement, the main contribution to ΔE_{tot} comes from stretching or compressing the B–B bonds—which, obviously, have very different energetic costs. In the calculations, the cubic anharmonicity of the mode is eliminated: after obtaining ΔE_{tot} with the displacements $+u$ and $-u$ we take an average, and are left with ΔE_{tot} carrying quartic anharmonicity only. Using the pattern (b) instead of (a) is technically somewhat simpler, because the averaging of the contributions from the stretched and compressed bonds is 'built in' within the same displacement pattern.

A striking feature of the $E_{2g}(\Gamma)$ mode (one which has already been noticed by other authors [9]) is its strong anharmonicity a_4; it is larger by an *order of magnitude* than that of the $B_{1g}(\Gamma)$ mode. This is equally true for the corresponding mode $E_{2u}(A)$ at the Brillouin zone boundary and, apparently, holds for the whole branch $E_{2g}(\Gamma)$–$E_{2u}(A)$. The ratio of the quartic energy to the square of the harmonic energy, for any given displacement u, is $a_4/a_2^2 = 4\ \mathrm{eV}^{-1}$ for $E_{2g}(\Gamma)$ and 3.5 for $E_{2u}(A)$. Yildirim *et al* [9] arrived at an even stronger anharmonicity of the $E_{2g}(\Gamma)$ mode: $a_4/a_2^2 \approx 8\ \mathrm{eV}^{-1}$.

Large anharmonicity is consistent with a strong variation of the phonon frequency with volume, and the mode Grüneisen parameters of $E_{2g}(\Gamma)$ and $E_{2u}(A)$ turn out to be much larger than those of the other modes (see table 2)—and, in any case, unusually large: 2.5 and 2.8, respectively. The corresponding frequency shifts $\Delta\omega \propto \gamma\omega$ are approximately the same, which means that the whole branch $E_{2g}(\Gamma)$–$E_{2u}(A)$ is shifting 'rigidly' when compressed—unlike the branch $B_{1g}(\Gamma)$–$B_{2u}(A)$ which becomes more dispersive under pressure.

It is interesting to note that for the $E_{2g}(\Gamma)$ and $E_{2u}(A)$ modes the quartic coefficient a_4 of equation (5) (not given in table 2) turns out to be approximately constant and independent of volume, over the entire range of volumes shown in figure 4; this means that, under pressure, the quartic energy goes as the inverse fourth power of the lattice constant a.

The anharmonic effect which is the most commonly observed in phonon spectroscopies is the broadening of the spectral features and their shift by some amount $\Delta(\omega)$ [42] with respect to the ideal $\delta(\omega' - \omega)$-like response of the perfectly harmonic system. A detailed treatment of the phenomena caused by anharmonicity would go beyond the scope of this work. As mentioned already, the two 'degenerate' modes $E_{2g}(\Gamma)$-(a) and $E_{2g}(\Gamma)$-(b) become, with finite displacements, two *inequivalent* patterns leading to different energies. In addition, one has to expect them to be coupled (phonon–phonon interaction).

If perturbation treatment is applied (up to the second order) to the *single* oscillators $E_{2g}(\Gamma)$-(a) and $E_{2g}(\Gamma)$-(b), then the cubic anharmonicity of the mode (a) makes the two frequencies slightly different: e.g. with the present values of a_2, a_3, a_4, the cubic anharmonicity cancels about 70% of the shift $\Delta(\omega)$ caused by the quartic term alone [43]. However, it is unclear whether the anharmonic terms of the present magnitudes are still amenable to perturbational treatment, and one can even question the validity of the entire concept of (nearly) independent modes.

An attempt (necessarily simplified) at treatment of the anharmonicity of the *isolated* $E_{2g}(\Gamma)$-(b) mode has been reported recently [9], within the self-consistent harmonic approximation [44], as well as by numerically solving the Schrödinger equation. Yildirim *et al* [9] estimated that (within the above-mentioned single-oscillator treatment) $\Delta(\omega)$ for the $E_{2g}(\Gamma)$-(b) mode amounts to a frequency shift by 17–25% above the harmonic frequency. That estimate is based on their results for a_2, a_4, $\omega(E_{2g}(\Gamma)) = 486\ \mathrm{cm}^{-1}$ and employs two different ways of calculating the effective frequency. Taking into account that the (relative) anharmonic shift, in the lowest order of perturbation theory, is proportional to the ratio a_4/a_2^2 and to the phonon energy $\hbar\omega$ itself [45], a simple rescaling of the Yildirim *et al* results suggests, for our case, a 9–13% upshift of the $E_{2g}(\Gamma)$ frequency; similarly, the shift in $E_{2u}(A)$ can be estimated at 7–10% (see the shaded areas in figure 4). Treating the calculated harmonic phonon frequencies in compressed unit cells in the same way, we estimate that these shifts reduce the Grüneisen parameters of the two modes from 2.5 and 2.8 to $\gamma_0 = 2.0$–2.2 and $\gamma_0 = 2.3$–2.5, respectively.

It is to be hoped that a more rigorous treatment of the anharmonic phenomena will soon provide more accurate results than these qualitative estimates.

3.5. Comparison with other calculations

There have been several calculations of zone-centre vibrations [6, 9, 21] and the phonon dispersion [8, 9, 22]. The results obtained for modes at Γ are compared in table 3. The most conspicuous feature of the comparison is the large spread of the results for the $E_{2g}(\Gamma)$ mode—the calculated frequency varies from $486\ \mathrm{cm}^{-1}$ [9] to $665\ \mathrm{cm}^{-1}$ [21]—although otherwise good agreement between different authors is found for the other Γ modes.

Table 3. Harmonic contributions to the phonon frequencies at the Γ point calculated by different *ab initio* methods. All frequencies are given in cm^{-1}.

$B_{1g}(\Gamma)$	$E_{2g}(\Gamma)$	$A_{2u}(\Gamma)$	$E_{1u}(\Gamma)$	Method	Reference
690	515	390	320	Frozen phonon	Kortus *et al* [6]
679	665	419	328	Linear response	Satta *et al* [21]
692	585	401	335	Linear response	Kong *et al* [8]
696	536	394	322	Linear response	Bohnen *et al* [22]; at V_0^{exp}
702	571	405	327	Linear response	Bohnen *et al* [22]; at V_0^{th}
702	486[a]	402	328	Frozen phonon	Yildirim *et al* [9]
695	535	400[b]	333[b]	Frozen phonon	Present work

[a] The frequency based on the harmonic term of the quadratic expansion of $\Delta E_{tot}(u)$ (analogous to equation (5)). The 'shifted' frequency obtained by treating the anharmonicity within the self-consistent harmonic approach or based on the energy levels of an anharmonic oscillator amounts to 565 or 601 cm^{-1}, respectively.

[b] Results obtained by fitting the calculated $E(u)$ with a *quadratic* polynomial.

Bohnen *et al* [22] attribute the disagreement in the frequency of the $E_{2g}(\Gamma)$ mode to an insufficiently converged $\vec{k}$-point sampling in some of the calculations. In our case we have ensured that full convergence is reached.

Large anharmonicity of $E_{2g}(\Gamma)$ was proposed as a possible cause of the discrepancies by Yildirim *et al* [9]. The proper 'separation' of the harmonic part in the calculated ΔE_{tot} does indeed matter: evaluating the frozen-phonon energy at $u = 0.057$ Å (=the r.m.s. displacement) we obtain, for the $E_{2g}(\Gamma)$-(a) mode, a harmonic term in equation (5) of 37.84 meV, a cubic term of 10.57 meV, and a quartic term of 5.33 meV. Adding the quartic contribution into the

harmonic energy would shift the frequency up by as much as 7%, assuming that the cubic term has been correctly eliminated (otherwise the frequency would be shifted by another ±14%).

When linear response theory is used for calculation of phonon frequencies the results are free of anharmonic contributions by construction. Nevertheless the results of references [8, 21, 22] for the $E_{2g}(\Gamma)$ mode show a large spread, too (cf. table 3).

We note that there is yet another factor which can be a source of considerable discrepancies. The large mode Grüneisen parameter implies a high sensitivity of the calculated $E_{2g}(\Gamma)$ phonon frequency to the (equilibrium) volume used. Some authors choose to perform the phonon calculations at the *experimental* equilibrium volume V_0^{exp} rather than at the *calculated* equilibrium volume V_0^{th}. Both choices are legitimate and, as a rule, choosing one rather than the other does not lead to any marked disagreement; the modes with large γ may nevertheless constitute an exception. Our present calculations refer to the *calculated* equilibrium value V_0^{th}, and the $E_{2g}(\Gamma)$ frequency at the experimental value V_0^{exp} would be only 12 cm^{-1} lower; the difference however becomes 35 cm^{-1} in reference [22] where the authors were careful enough to determine *two* sets of frequencies for all Γ-point phonons, namely one at the theoretical and one at the experimental equilibrium value. Generally, the existence of two results (one at V_0^{th} and one at V_0^{exp}) is an intrinsic uncertainty underlying the concept of frozen phonons itself [46] and, in a sense, it can be thought of as a consequence of the DFT-LDA. If we estimate that, in a typical DFT-LDA calculation, V_0^{th} is between 1% and 3% under the experimental value V_0^{exp}, and with the Grüneisen parameter of the order of $\gamma = 2.5$, the two calculations of frequencies of $E_{2g}(\Gamma)$ can differ by as much as 2.5% to 7.5% (≈40 cm^{-1}).

Other possible sources of discrepancies between frozen-phonon results are the errors of statistical nature that relate to the details of the fitting of equation (5), e.g., the choice of the degree of the polynomial and the selection of the displacements u for which the $E(u)$s are calculated and the polynomial then fitted. Even if the consequent differences are relatively small, the choices should be clearly stated for the sake of reproducibility.

The $E_{2g}(\Gamma)$ mode is, apparently, very sensitive to all details of the calculation. Besides the convergence with the plane-wave cut-off, the $\vec{k}$-point sampling, and the technique used for dealing with the incompletely filled orbitals (the 'metallic sampling' algorithm)—which are amenable to quantitative testing—yet another source of divergences between different calculations is in the choice of the pseudopotentials or of the method for determination of the total energy. The consequent uncertainties are difficult to estimate though.

Considering the large spread, among different authors, in the calculated values of the $E_{2g}(\Gamma)$ mode frequencies, experimentally, one might attempt to discern this mode from the others by its unusually large value of the Grüneisen parameter γ rather than by its frequency.

3.6. Mode Grüneisen parameters and pressure dependence of T_c

The whole optical phonon branch connecting the $E_{2g}(\Gamma)$ and the $E_{2u}(A)$ modes was shown to exhibit strong electron–phonon coupling [8, 22]. Within an intermediate- or strong-coupling scenario it is considered to largely determine the superconducting properties of MgB_2. Based on early calculations of the electron–phonon coupling constant $\lambda \approx 0.7$, an assumed mode Grüneisen parameter $\gamma = 1$, and a calculated pressure dependence of the density of states at the Fermi level of $\mathrm{d}\ln N(0)/\mathrm{d}P = -0.31\%\ \mathrm{GPa}^{-1}$, the pressure dependence $\mathrm{d}\ln T_c/\mathrm{d}P$ of the critical temperature was estimated to fall in the range −2.3 to −3.6% GPa^{-1} [20]. The estimate compared well with experimental data and thus supported the notion of BCS superconductivity in MgB_2. The pressure-induced increase in characteristic phonon frequency was identified as the dominant cause of the decrease of T_c under pressure.

With a refined calculated value of $\lambda = 0.87$ [8], $\omega_0 = 500$ cm^{-1}, and a typical Coulomb pseudopotential of $\mu^* = 0.1$, we obtain $T_{c,P=0} = 36.7$ K based on the McMillan expression in the form given in reference [20]. Following the analysis of reference [20] but using an average $\gamma = 2.3$ for the $E_{2g}(\Gamma)$–$E_{2u}(A)$ phonon branch (taking into account anharmonicity) and a bulk modulus $B_0 = 145$ GPa as calculated above, as well as $\mathrm{d}\ln N/\mathrm{d}P = -0.31\%$ GPa^{-1} [20], we estimate $\mathrm{d}T_c/\mathrm{d}P \approx -1.8$ K GPa^{-1}. Experimental values of $\mathrm{d}T_c/\mathrm{d}P$ in the range -0.7 to -2.0 K GPa^{-1} have been reported [10–14]. The large spread of experimental data was, at least in part, attributed to differences in the samples studied [14]. Our estimate of the pressure dependence of T_c is close to the upper limit of the range of experimental values. This, however, is not surprising because we used the large Grüneisen parameter of the dominant $E_{2g}(\Gamma)$–$E_{2u}(A)$ phonon branch. Non-negligible contributions from other vibrational modes with smaller pressure dependences are expected to reduce the pressure shift of T_c compared to our estimate.

Other effects may also be of relevance, especially a possible pressure dependence of the electron–ion matrix element I which enters the electron–phonon coupling constant λ and was assumed to be constant here. Nevertheless, the present results (in particular the large mode Grüneisen parameter of the phonon branch with the strongest electron–phonon coupling) underline the dominant role of the pressure dependence of the phonon spectrum with regard to T_c.

4. Experiments

4.1. Experimental details

Polycrystalline MgB_2 was prepared from stoichiometric mixtures of Mg (Johnson-Matthey Incorporated, 99.98%) and natural boron powder (-325 mesh, 99.99%, Aldrich). The reaction was carried out at 850 °C for two days using sealed Ta capsules under Ar atmosphere that were in turn encased in evacuated silica tubes. After grinding under Ar, the sample was annealed at the same temperature for one day. The x-ray powder diffraction pattern showed a single-phase sample with $a = 308.63(3)$ pm and $c = 352.34(3)$ pm. In susceptibility measurements the superconducting transition was observed at $T_c = 38.2(1)$ K.

For the high-pressure experiments at ambient temperature small amounts of the powder samples were placed into gasketed diamond anvil cells (DACs). The remainder of the sample cavity was filled with KCl as a quasi-hydrostatic pressure medium. The sample was in direct contact with the diamond window through which the Raman and reflectance spectra were taken.

High-pressure Raman spectra were excited at 633 nm employing a long-distance microscope objective. They were recorded in back-scattering geometry using a single-grating spectrometer with a multi-channel CCD detector and a holographic notch filter for suppression of the laser line (Dilor LabRam). For the Raman experiments the DAC was equipped with synthetic diamonds (Sumitomo type IIa) which emit only minimal luminescence. Optical reflectivity spectra of MgB_2 in the energy range 0.6–4.0 eV were measured using a micro-optical set-up described in reference [47]. Pressures were measured by the ruby luminescence method [48, 49]. Low-temperature Raman spectra of MgB_2 were excited with the 647 nm line of a Kr-ion laser. The scattered light was analysed by a triple-grating spectrometer (Jobin-Yvon T64000) in combination with a multi-channel CCD detector. A DAC with synthetic diamonds was used as a low-luminescence container for the powder sample.

4.2. Optical reflectance under pressure

We first take a brief look at the optical reflectance spectra of MgB_2, because they provide some information that helps one to understand the evolution of the Raman spectra under pressure. At low pressures, a low reflectance is observed throughout the spectral range from 0.6 to 4 eV (figure 5(a)). At higher pressures the NIR reflectance increases and above 10 GPa we observe a Drude-like edge characteristic of a metallic sample. This edge then remains present even upon pressure release from 25 to 1 GPa. This observation indicates that the grains of the MgB_2 powder may be covered with some non-metallic surface layer which is, at least partially, removed by the deformation of the grains upon compression. X-ray photoemission studies have indeed shown that MgB_2 samples which have been exposed to air are covered with surface layers of B_2O_3 [50] and possibly $MgCO_3$ or $Mg(OH)_2$ [51]. Werheit *et al* concluded that samples of boron-rich compounds in general tend to be covered with surface contaminants which are not transparent near 500 nm [52]. Consequently, Raman spectra of such compounds excited in the visible spectral region may be dominated by contributions from the surface layer rather than the bulk material.

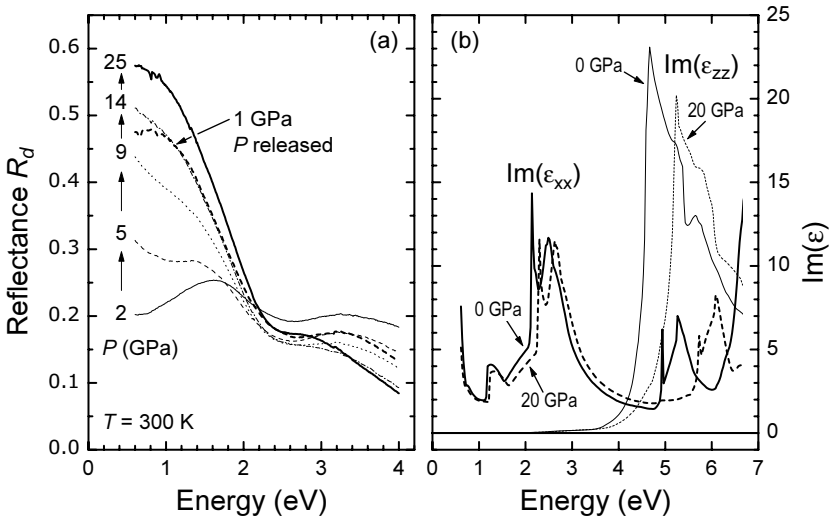

Figure 5. (a) Optical reflectance spectra of MgB_2 at ambient temperature and pressures up to 25 GPa. R_d denotes the absolute reflectance at the diamond–sample interface. (b) The calculated imaginary part of the dielectric function (interband transitions) at 0 GPa (solid lines) and 20 GPa (broken lines) for light polarized perpendicular (ε_{xx}) and parallel (ε_{zz}) to the c-axis.

The energetic position of the Drude edge uncovered by pressure cycling is probably determined by the onset of strong interband absorption at energies around 2 eV. The fact that the edge shows a small red-shift of less than 10 meV GPa^{-1} on releasing the pressure from 25 to 1 GPa indicates a small change of the related interband absorption threshold. We have calculated the interband contributions $\varepsilon_{xx}(\omega)$ and $\varepsilon_{zz}(\omega)$ to the imaginary part of the dielectric function of MgB_2 (see figure 5(b)) using the WIEN97 code [53] with parameters as described in reference [20]. Without going into details here, we just note that the calculated $\varepsilon_{xx}(\omega)$ indeed shows a threshold at 2.1 eV, which shifts under pressure to higher energy at a rate of 8 meV GPa^{-1}. These interband transitions may result in resonance effects in Raman scattering.

4.3. Raman spectra under pressure

Figure 6 shows ambient-temperature Raman spectra of MgB_2 recorded at increasing pressures in the range 0–14 GPa and decreasing pressures of 15–0 GPa. In between, the pressure was increased to ∼20 GPa. The 0.6 GPa spectrum of figure 6(a), consisting of a broad peak near 600 cm^{-1} with a high-energy shoulder, is representative of the ambient-pressure Raman spectra of numerous samples that we have investigated. It is also quite similar to an ambient-pressure Raman spectrum of MgB_2 reported by Bohnen *et al* [22]. With increasing pressure the shoulder gains intensity and the spectrum exhibits two clearly resolved peaks. The enhanced intensity of the higher-energy peak persisted upon pressure release until the cell was opened and the sample was exposed to air (figure 6(b)).

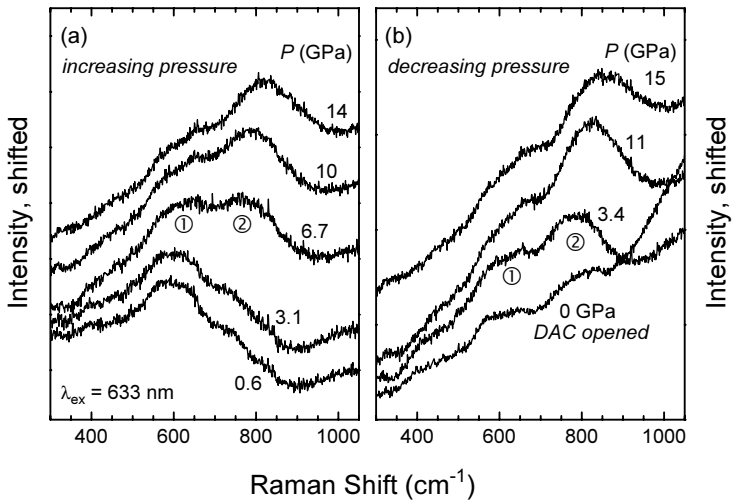

Figure 6. Raman spectra of MgB_2 for (a) increasing and (b) decreasing pressures ($T = 300$ K). In between, the pressure was increased to ∼20 GPa. After pressure release the sample was in contact with air before the 0 GPa spectrum in (b) was recorded.

Neither of the observed peaks can be attributed to the Raman-active $E_{2g}(\Gamma)$ mode or to the silent $B_{1g}(\Gamma)$ mode. The observed pressure-induced peak shifts (figure 7, table 4) translate to mode Grüneisen parameters of $\gamma_1 = 0.27$–0.45 and $\gamma_2 = 0.8$–1.2 for peaks (1) and (2), respectively, using $B_0 = 145$ GPa. Hence, the calculated Grüneisen parameter of the $E_{2g}(\Gamma)$ phonon and the experimental value for peak (1) differ by a factor of ∼6. Similarly, for peak (2) the mode Grüneisen parameter and the 0 GPa frequency differ by factors of 2.3 and >200 cm^{-1}, respectively, from the values calculated for the $E_{2g}(\Gamma)$ mode. The pressure-induced peak shifts appear not to be fully reversible. This may, at least in part, be attributed to difficulties in determining the exact peak positions because of an intense non-linear background that changes with pressure. It does not, however, compromise the above conclusion.

Tentatively, we attribute the higher-energy mode (2) with $\omega_0 = 750 \pm 20$ cm^{-1} to a well-defined peak in the phonon density of states near 730 cm^{-1} according to calculations by Kong *et al* [8] and Bohnen *et al* [22] as well as inelastic neutron scattering data by Osborn *et al* [23]. Observation of this density-of-states peak in our spectra implies a violation of the momentum conservation for the Raman scattering process which may originate from disorder of the sample and/or the small optical penetration depth of the laser light into the *metallic* sample. A violation of the momentum conservation would not lead to spectral features near the frequency of the $E_{2g}(\Gamma)$ mode, as there is no density-of-states peak at this frequency [8,22].

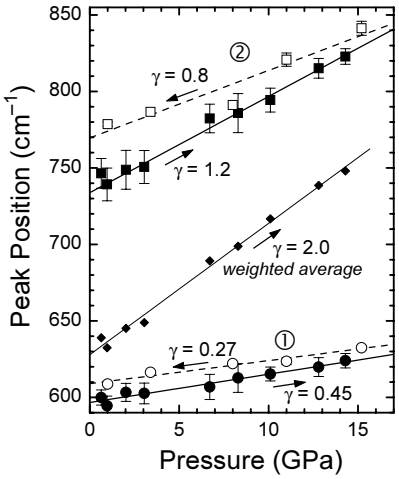

Figure 7. Energies of the Raman features (1) and (2) of MgB_2 as a function of pressure. Solid and open symbols refer to data measured with increasing and decreasing pressures, respectively. Lines represent linear relations fitted to the data.

Table 4. Observed frequencies ω_0 of Raman features of MgB_2 and their pressure coefficients $a = \mathrm{d}\omega/\mathrm{d}P$. The values for the mode Grüneisen parameters γ_0 are based on a bulk modulus $B_0 = 145$ GPa.

Mode		ω_0 (cm^{-1})	a (cm^{-1} GPa^{-1})	γ_0
Peak (1)	P up	597(1)	1.85(15)	0.45
	P down	609(2)	1.51(19)	0.27
	Up/down average	603(6)	1.68(17)	0.40
Peak (2)	P up	734(3)	6.3(3)	1.2
	P down	770(8)	4.4(8)	0.8
	Up/down average	752(18)	5.4(10)	1.0

Taking into account the observations made from reflectance measurements, we conclude that only the higher-energy peak (2) in our Raman measurements originates from MgB_2 which is uncovered from surface layers through the application of high pressure. The lower-energy peak (1) which is the dominant feature of the Raman spectra of MgB_2 at ambient conditions is attributed to a surface layer of different chemical composition. It should be noted that we observed this mode also for samples that had been stored under inert conditions. Probably the surface layers had formed already during the material synthesis.

Goncharov *et al* have also studied MgB_2 at high pressures by Raman spectroscopy [19]. In contrast to our results they observed only a single broad spectral feature (FWHM: $\sim$300 cm^{-1}) centred near 620 cm^{-1} (at 0 GPa) showing a large pressure dependence ($\gamma = 2.9$). They assign the feature to first-order Raman scattering, but also consider other possible interpretations. Their observations may be reconciled with ours if one assumes that the two components visible in our spectra (FWHM: $\sim$180 cm^{-1}) contribute to the very broad spectral feature observed by Goncharov *et al*. The change in the relative intensities of the components (1) and (2) would then lead to a large pressure dependence of the 'smeared-out' peak. The weighted average ('centre of gravity') of the two peak positions exhibits an effective Grüneisen parameter $\gamma = 2.0$ (figure 7). A direct interpolation between peak (1) at 0 GPa and peak (2) at 14 GPa results in

$\gamma = 4.0$. The resulting range for the effective γ of 2.0–4.0 thus includes the value $\gamma = 2.9$ given in reference [19].

4.4. Low-temperature Raman spectra

We investigated whether it is possible to observe a pair-breaking excitation below T_c similar to what has been reported for conventional superconductors such as Nb_3Sn and V_3Si [54].

Upon cooling of a MgB_2 sample below 50 K we observed a build-up of additional scattering intensity in the range 50–300 cm^{-1} (figure 8(a)) which can be modelled by two Gaussian peaks located at 128 and 226 cm^{-1}, respectively, in the 2 K spectrum. These peak positions are higher in energy than $2\Delta_0 \approx 90$ cm^{-1} according to BCS theory, i.e. $2\Delta_0 \approx 3.5 k_B T_c$ with $T_c = 38$ K. A number of experiments, however, have indicated superconductivity in MgB_2 to be in the intermediate- or strong-coupling regime with $2\Delta_0/k_B T_c$ up to 5 ($2\Delta_0 \approx 130$ cm^{-1}) [55]. With increasing temperature these peaks vanish only at a temperature between 74 and 100 K, i.e., well above T_c (figure 8(b)). They were observed only for parallel polarizations of the incident and scattered light. Furthermore, the rising intensity below 30 cm^{-1} is not due to residual stray light but originates from Raman scattering by the sample. The physical origin of the spectral features reported is unclear at present.

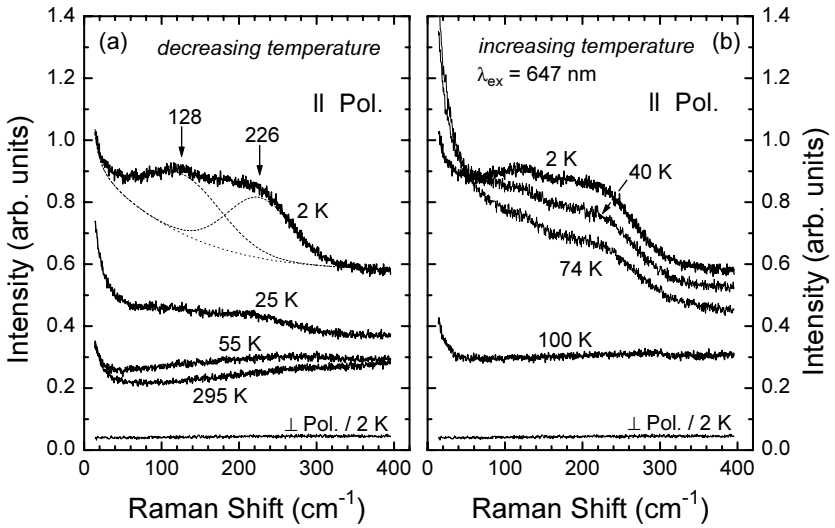

Figure 8. Raman spectra of MgB_2 at ambient pressure for (a) decreasing and (b) increasing temperatures. '∥ Pol.' and '⊥ Pol.' refer to parallel and crossed polarizations of the incident and scattered light, respectively.

Chen *et al* also investigated the superconducting gap of MgB_2 by Raman spectroscopy [25]. They reported a redistribution of spectral weight at frequencies below ∼200 cm^{-1} and the appearance of a small peak at 110 cm^{-1} which they attributed to the pair-breaking excitation. At variance with our results, a polarization dependence of the Raman spectra was not observed.

5. Conclusions

Using the frozen-phonon approach we have calculated the harmonic frequencies of selected optical phonons of MgB_2 for different volumes corresponding to a pressure range of 0 to

30 GPa. Large differences are found in the absolute values of mode Grüneisen parameters. In particular, for the whole $E_{2g}(\Gamma)$–$E_{2u}(A)$ branch the frequencies are highly sensitive to volume changes, as indicated by large values of the corresponding mode Grüneisen parameters. In earlier calculations [8, 22] the $E_{2g}(\Gamma)$–$E_{2u}(A)$ branch of the phonon dispersion was identified as the one which exhibits the strongest electron–phonon coupling. Therefore, within an intermediate- or strong-coupling scenario it is considered to govern the superconducting properties of MgB_2. Within this picture the present results for the mode Grüneisen parameters underline the dominant role of the phonon spectrum with respect to the observed decrease of T_c with pressure.

On the basis of our calculations and Raman scattering experiments on MgB_2 at high pressures we conclude that the dominant Raman peak near 600 cm^{-1} in the ambient-pressure spectra reported by various authors does not originate from MgB_2. We relate it instead to a contaminant phase present at the sample surface. A second peak located near 750 cm^{-1}, visible only as a weak shoulder in spectra of as-grown samples, is tentatively attributed to a peak in the phonon density of states. A calculation of the phonon density of states *under pressure*, extending previous ambient-pressure work [8, 22], is desirable to test this assignment.

Temperature-dependent Raman experiments on MgB_2 showed a build-up of additional scattering intensity in the region below 300 cm^{-1} upon cooling below T_c. A broad double-peak structure appeared at 130/230 cm^{-1} and vanished only upon warming the sample to temperatures well above T_c. Further study of the low-temperature Raman spectra of MgB_2 is clearly needed to elucidate the physical origin of the various observations.

Acknowledgments

We acknowledge useful discussions with R Zeyher. The computer resources used in this work were provided by the Scientific Committee of IDRIS, Orsay (France).

References

[1] Nagamatsu J, Nakagawa N, Muranaka T, Zenitani Y and Akimitsu J 2001 *Nature* **410** 63
[2] Bud'ko S L *et al* 2001 *Phys. Rev. Lett.* **86** 1877
[3] Rubio-Bollinger G, Suderow H and Vieira S 2001 *Phys. Rev. Lett.* **86** 5582
[4] Karapetrov G *et al* 2001 *Phys. Rev. Lett.* **86** 4374
[5] Sharoni A, Felner I and Millo O 2001 *Phys. Rev.* B **63** 220508(R)
[6] Kortus J *et al* 2001 *Phys. Rev. Lett.* **86** 4656
[7] An J M and Pickett W E 2001 *Phys. Rev. Lett.* **86** 4366
[8] Kong Y, Dolgov O V, Jepsen O and Andersen O K 2001 *Phys. Rev.* B **64** 020501(R)
[9] Yildirim T *et al* 2001 *Phys. Rev. Lett.* **87** 037001
[10] Saito A *et al* 2001 *J. Phys.: Condens. Matter* **13** L267
[11] Monteverde M *et al* 2001 *Science* **292** 75
[12] Lorenz B, Meng R L and Chu C W 2001 *Phys. Rev.* B **64** 012507
[13] Tomita T *et al* 2001 *Phys. Rev.* B **64** 092505
[14] Lorenz B, Meng R L and Chu C W 2001 *Phys. Rev.* B **64** 012507
[15] Ahn K, Gibson B J and Kremer R K, unpublished results
[16] Vogt T *et al* 2001 *Phys. Rev.* B **63** 220505
[17] Prassides K *et al* 2001 *Phys. Rev.* B **64** 012509
[18] Jorgensen J D, Hinks D G and Short S 2001 *Phys. Rev.* B **63** 224522
[19] Goncharov A F *et al* 2001 *Phys. Rev.* B **64** 100509
[20] Loa I and Syassen K 2001 *Solid State Commun.* **118** 279
[21] Satta G *et al* 2001 *Phys. Rev.* B **64** 104507
[22] Bohnen K-P, Heid R and Renker B 2001 *Phys. Rev. Lett.* **86** 5771
[23] Osborn R, Goremychkin E, Kolesnikov A and Hinks D 2001 *Phys. Rev. Lett.* **87** 017005

[24] Sato T J, Shibata K and Takano Y 2001 *Preprint* cond-mat/0102468
[25] Chen X *et al* 2001 *Phys. Rev. Lett.* **87** 157002
[26] Martinho H *et al* 2001 *Preprint* cond-mat/0105204v2
[27] Hlinka J *et al* 2001 *Preprint* cond-mat/0105275
[28] Perdew J P and Wang Y 1992 *Phys. Rev.* B **45** 13 244
[29] Kresse G and Hafner J 1993 *Phys. Rev.* B **47** R558
[30] Kresse G 1993 *PhD Thesis* Technische Universität Wien
[31] Kresse G and Furthmüller J 1996 *Comput. Mater. Sci.* **6** 15
[32] Kresse G and Furthmüller J 1996 *Phys. Rev.* B **54** 11 169
[33] Vanderbilt D 1990 *Phys. Rev.* B **41** 7892
[34] Kresse G and Hafner J 1994 *J. Phys.: Condens. Matter* **6** 8245
[35] Louie S G, Froyen S and Cohen M L 1982 *Phys. Rev.* B **26** 1738
[36] Jepsen O and Andersen O K 1971 *Solid State Commun.* **9** 1763
[37] Blöchl P E, Jepsen O and Andersen O K 1994 *Phys. Rev.* B **49** 16 223
[38] Murnaghan F D 1944 *Proc. Natl Acad. Sci. USA* **50** 244
[39] Pearson W B 1979 *Proc. R. Soc.* A **365** 523
[40] Bräuninger S, Schwarz U and Syassen K, unpublished
[41] Yin M T and Cohen M L 1980 *Phys. Rev. Lett.* **45** 1004
Kunc K and Martin R M 1981 *Phys. Rev.* B **24** 2311
[42] Cowley R A 1968 *Rep. Prog. Phys.* **31** 123
[43] Landau L D and Lifshitz E M 1976 *Mechanics* 3rd edn (Oxford: Pergamon) equation (28.13)
[44] See, e.g., Brüesch P 1982 *Phonons: Theory and Experiments I* (Berlin: Springer) section 5.4
[45] Kunc K and Zeyher R 1994 *Phys. Rev.* B **49** 12 216
[46] Needs R J, private communication
[47] Goñi A R and Syassen K 1998 *High Pressure in Semiconductor Physics I (Semiconductors and Semimetals vol 54)* ed T Suski and W Paul (New York: Academic) p 248
[48] Piermarini G J *et al* 1975 *J. Appl. Phys.* **46** 2774
[49] Mao H K, Xu J and Bell P M 1986 *J. Geophys. Res.* **91** 4673
[50] Callcott T A *et al* 2001 *Preprint* cond-mat/0103593
[51] Vasquez R P *et al* 2001 *Phys. Rev.* B **64** 052510
[52] Werheit H *et al* 1999 *J. Alloys Compounds* **291** 28
[53] Blaha P, Schwarz K and Luitz J 1999 *WIEN97: a Full Potential Linearized Augmented Plane Wave Package for Calculating Crystal Properties* Karlheinz Schwarz, Technische Universität Wien, Austria (ISBN 3-9501031-0-4)
[54] Dierker S B, Klein M V, Webb G W and Fisk Z 1983 *Phys. Rev. Lett.* **50** 853
[55] Kotegawa H *et al* 2001 *Phys. Rev. Lett.* **87** 127001